Trends in reactivity of electrodeposited 3d transition metals on gold revealed by *operando* soft X -ray absorption spectroscopy during water splitting

J. J. Velasco-Vélez[1,2]*, Travis E. Jones[1], Verena Pfeifer[1], Chung-Li Dong[3,4], Yu-Xun Chen[3], Chieh-Ming Chen[3], Hsin-Yu Chen[3], Ying-Rui Lu[3], Jin-Ming Chen[4], R. Schlögl[1,2], A. Knop-Gericke[1], C.-H. Chuang[3,*]

Corresponding authors: velasco@fhi-berlin.mpg.de, and chchuang@mail.tku.edu.tw

[1]Department of Heterogeneous Reactions, Max Planck Institute for Chemical Energy Conversion, Mülheim an der Ruhr 45470, Germany

[2]Department of Inorganic Chemistry, Fritz-Haber-Institut der Max-Planck-Gesellschaft, Berlin 14195, Germany

[3]Department of Physics, Tamkang University,New Taipei City 25137, Taiwan.

[4]National Synchrotron Radiation Research Center, Hsinchu 30076, Taiwan

Abstract: We activated gold electrodes for their use as electrocatalyst for water splitting by electrodepositing Cu, Ni and Co. A combination of *operando* X-ray absorption spectroscopy and potentiometric control under aqueous conditions revealed the trends in reactivity yielded by these electrodes, which are directly associated with the cross- and overpotentials as well as the occupancy of the 3d orbitals. It was found that under anodic polarization the materials electrodeposited on gold suffer from a lack of stability, while under cathodic polarization they exhibit stable behavior. The observed activity is strongly related to the lack of stability shown by these composites under anodic polarization revealing a dynamic process ruled by corrosion. By *operando* X-ray absorption, we established that the overall enhancement of the activity for the oxygen evolution reaction is directly attributable to the cross-potential and corrosion process of the electrodeposited materials. It is associated with the high potential deposition, which is the origin of the incipient oxidation-corrosion resistance of the lattice. We conclude that the observed trends in the total current are directly associated with the loss of oxygen in the metal-oxide lattice and the subsequent dissolution of metallic ions in the electrolyte under anodic polarization.

1. Introduction

Fabrication of electrodes for efficient chemical energy conversion by water splitting to molecular hydrogen and oxygen is of prime importance. In particular the decrease of energy losses and the increase of the stability of such materials are the current focus of many studies. The anodic half reaction, the OER, is by far the most complex process which is limited by the high electrode overpotential and the lack of stability. Gold has poor electrocatalytic performance as a water splitting catalyst due to its inability to activate one of the most important steps of the reaction, the breaking of O-H bonds in the dissociation of water ($H_2O \rightarrow OH^- + H^+$) [1]. The relatively large energetic barrier can be overcome by using oxygen species on Au to facilitate the formation of OH at low temperatures [2]. However, the inability of Au to replace the

reacted O prevents a sustainable catalytic process. The addition of a small amount of metal-oxide, such as titanium or cerium oxides, on top of the Au surface facilitates this rate-determining step and easily continues the catalytic cycle of the production of O_2. Despite this activation strategy bulk Au is a very poor catalyst, but Au nanoparticles on metal oxide [3] and carbide [4] materials show unusual catalytic properties. For example, it has been shown that CeO_2 NPs smaller than 10 nm dispersed on Au are an excellent catalyst for the water gas shift reaction [5]. In addition, controlling the partial coverage of Au with TiO_2 or CeO_2 enhances the catalytic activity [6]. Thus, role of size of different Au NPs has been shown as important factor in the catalytic activity [7]. Ideally, one can take advantage of these phenomena and develop highly efficient catalysts by optimizing the Au/metal-oxide synergy. Electrodeposition is an attractive method used to deposit a large variety of materials [8] and allows for precise control of the chemical composition and the structure of the electrodeposited material. However, not all the materials can be electrodeposited in aqueous environment like the alkali metals. Decoding the structure of the electrodeposited electrode, requires the use of advanced spectroscopic methods capable of providing detailed information about the electronic structure of polarized solid-liquid interfaces [9]. *Ex-situ* studies are unable to describe such complex electrochemical processes since the chemical reactions are often rather unique and cannot be “quenched” and investigated by “post-mortem” studies [10]. X-ray spectroscopy is a powerful element specific technique that allows for an unequivocal assignment of chemical species. Almost all X-ray spectroscopic techniques yielding insights into the electronic structure require a vacuum environment, which is hardly compatible with liquids, especially water. Therefore, these investigations are still technologically challenging. These limitations can be overcome by using photon-in/photon-out (PIPO) techniques in the soft X-ray range with an information depth of a few hundred nanometers [11]. Thus, they enable the study of liquids in thermodynamic equilibrium at environmental pressure, i.e. in the liquid phase. In the past, a liquid flow cell was designed using a thin, liquid-tight SiN_x membrane (100 nm thick) to separate the UHV environment from the aqueous medium which was used for investigate the electrochemical oxidation of Cu [12].

The trends in activity for the HER and the OER of complex systems were revealed in previous investigations [13-21], which shown a huge discrepancy between different studies. However, the corrosion role (stability) of these materials has to be considered in the overall system performance as well [22] and has been neglected systematically in a multitude of electrochemical characterizations. Using a combination of *operando* X-ray absorption spectroscopy (XAS) and potentiometric control, we reveal, in the present contribution, the electronic structure of electrodeposited Cu, Ni and Co on Au. We find that the trend in activity under anodic polarization can be ascribed to the lack of stability shown by the metal-oxides. Therefore, we confirm that the electrodeposited transition metals act as sacrificial layers under anodic polarization and not as catalysts because they are consumed during the process, which reduces the overpotential in the oxygen evolution reaction (OER) enhancing the total process

current until they are depleted. The trends in activity show a clear correlation with the cross-potential, which is related to the equilibrium potential of the metal redox couple, indicating that the transition metals deposited at more negative potentials are more active but less stable, which can be ascribed in addition to their metal novelty. On the other hand, these electrodes featured good stability and corrosion resistance under cathodic polarization, which makes them ideal catalysts for reduction reactions, i.e. hydrogen evolution reaction (HER) or cathodic CO_2 reduction. The preparation of more stable electrodeposited catalysts for the OER remains a challenge and will require an upgrade of our electrochemical approach to allow thermal treatments to create more stable oxides and investigate the variation in the electronic structure under such conditions.

2. Methods

2.1 Experimental

Figure 1 shows a photograph (including the detection scheme) of the experimental setup commissioned at the beamline 20A1 of the National Synchrotron Radiation Research Center (NSRRC) in Hsinchu, Taiwan. Using this setup, it is possible to monitor the electronic structure of the working electrode under reaction conditions. The X-ray photons penetrate the thin SiN_x membrane (100 nm) and the working electrode [12-14]. Photons generated on the back side are detected in FY mode yielding information about the electronic structure of the growing layer under reaction conditions in an aqueous environment. The thin electrodeposited metal-oxide material does not suffer from self-absorption effects due to its thinness [15]. Using a Cressington 208 HR sputter coater, a thin film of Au (20 nm) was sputtered on internal side of the SiN_x membrane and was used as a working electrode. The sputtered thin film covers the whole membrane and presents a polycrystalline structure with a roughness in the order of ~10 nm as the AFM measurement in contact mode in Figure 1 proves and a dominant Au[111] orientation as the XRD measurements indicated. The electrochemical setup was completed by platinum counter and pseudo-reference electrodes. The thin electrodeposited films were obtained by cathodic deposition of copper, cobalt and nickel ions using three different electrolytes prepared by diluting 0.978 g of $CuSO_4$, 0.774 g of $NiSO_4$ and 0.775 g of $CoSO_4$ (Sigma Aldrich) in 1 litre of ultrapure Milli-Q water yielding a 5 mM concentration for the three electrolytes. After that, the electrochemical performance of these electrodes was investigated with a potentiostat (VersaSTAT4, Princeton Applied Research) using 10 mM KCl (Sigma Aldrich). This electrolyte was selected to minimize the influence of OH^- and H^+ species present in alkaline and acidic electrolytes, respectively. To support the spectroscopic measurements, the surface

morphology modifications were observed by *operando* electrochemical scanning tunneling microscopy (EC-STM) measurements performed with a Veeco Multi-Mode NanoScope equipped with an electrochemical STM cell.

2.2 Computational Approach:

Density functional theory (DFT) calculations were performed using the Perdew, Burke, and Ernzerhof (PBE) approximation for the exchange and correlation potential [27] with the Quantum ESPRESSO package [28]. The electron-ionic core interactions were represented by ultrasoft pseudopotentials taken from the PS library [29]. The Kohn-Sham states were expanded with a plane-wave basis set using a kinetic energy (charge density) cutoff of 30 Ry (300 Ry).

The Au/oxide interfaces were modeled using a Au(111) surface with 5-layers, where the bottom two layers were fixed at their bulk values during geometry optimizations. The lattice constant was fixed to the computed bulk value of gold (4.18 Å). Slabs were separated from their periodic images with approximately 15 Å of vacuum and a **k**-point mesh equivalent to (12x12) for the (1x1) surface unit-cell was employed. Marzari-Vanderbilt cold smearing was used with a smearing parameter of 0.001 Ry [30].

In separate calculations we placed four layer slabs of Cu_2O, NiO, and Co_3O_4, with a (111) surface termination, on a (2x2) Au(111) surface. Restricting the lattice constant of the underlying gold slab required a 4% and 2% compression of the Cu_2O and NiO surfaces with respect to their computed bulk lattice constants, respectively; whereas the Co_3O_4 surface had to be expanded by 2% to make it commensurate with the gold surface.

Calculations on Cu_2O were performed without spin polarization, whereas calculations on the other two oxides were performed with anti-ferromagnetic ordering of the Ni^{2+} and Co^{2+} ions in the [111] direction normal to the surface. Furthermore, an on-site Coulomb repulsion term (U) was added to account for the incomplete cancellation of the Coulomb self-interaction afforded by the PBE approximation [31], which is needed for an accurate description of NiO and Co_3O_4 [31, 32]. This term was computed for both bulk NiO and Co_3O_4 from linear response [31]. For Co_3O_4 we found U values of 5.28 eV for the non-magnetic octahedrally coordinated Co^{3+} ions and 4.32 eV for the magnetic tetrahedrally coordinated Co^{2+} ions. For Ni we computed a U of 6.47 eV. For simplicity we made no attempt to compute U on the atoms at the interface. Instead, we employed these bulk values in all calculations.

The adhesion energy of the oxide on the underlying gold was computed as:

$$E_{ad} = \frac{1}{A}\left(E_{Au/oxide} - E_{Au} - E_{oxide}\right)$$

where A is the surface area of the (2x2) Au(111) surface, $E_{Au/oxide}$ is the total energy of

the Au/oxide system and E_{Au}-E_{oxide} is the total energy of the 5 layer gold slab (4 layer oxide slab) alone, where the same computational cell and **k**-point mesh was used in all simulations. Here the sign convention is chosen negative, that is, more negative corresponds to more strongly bound oxides.

3. Results

3.1 Electrodeposition of 3d transitions metals on Au

Using the setup shown in Figure 1, $CuSO_4$, $NiSO_4$ and $CoSO_4$ solutions (5 mM, prepared in ultrapure Milli-Q water) were flowed in the cell to investigate the overpotential electrodeposition of such transition metal ions on the Au working electrode. Electrochemical deposition involves the reduction of metal ions from an aqueous solution onto a foreign substrate. During the layer formation, several steps such as diffusion of electroactive species, loss of solvation shell and formation/incorporation of ad-atoms to the lattice site can occur. These processes are driven by the coordination sphere of the metals ions, which determines the nucleation [33]. Figure 2 shows the cyclic voltammograms (CV) recorded at 20 mV/s with continuous flows of 5 mM of $CuSO_4$, $NiSO_4$ and $CoSO_4$, respectively. The CVs show cross-potentials (V_C) of -0.4 V for copper, -0.5 V for nickel and -0.9 V for cobalt, indicating the equilibrium potential of the metal redox couple ascribed to the metal/metal-ion reversible potential [34].

The overpotential depositions of copper, nickel and cobalt were accomplished at V_d (deposition potential) -0.5 V, -0.6 V and -1.0 V, respectively, as shown Figure 2. The total charge transferred during the electrodeposition was 500 μC that correspond to a thickness of around 100 nm for these materials. Subsequently the electrodes were conditioned for 5 minutes by continuous potential cycling between -1 V and +1 V at 20 mV/s in 10 mM KCl. The potential was stopped at open circuit voltage (OCV). Holding the electrode potential at a positive bias respect to the point of zero charge induce the formation of unreconstructed terraces, which can be reconstructed under negative polarization [35]. This effect is so-called electrochemical annealing [36]. The electronic structure of the electrodeposited material was monitored online by means of FY-XA spectroscopy recorded at several polarization biases. The XA spectra provide direct insight into the electronic transitions from core levels to unoccupied final states of the target element, enabling spectroscopic identification of chemical species. Figures 2a, 2b and 2c show the Cu, Ni and Co L_{II-III}-edges spectra of the electrodeposited materials as a function of charge elapsed. $L_{II,III}$-edges in transition metal oxides are dominated by the excitation of 2p electrons to the unoccupied 3d states. Therefore, XAS can elucidate the electronic structure and the coordination environment of these complex electrodes. Figure 2a shows the CV of the electrodeposited Cu as well as the XA spectra as a function of time. These spectra feature intense peaks at 932 eV (L_{III}) and 952 eV (L_{II}) ascribed to the formation of Cu_2O species (Cu^+) [12]. Otherwise, Figure 2b shows the spectra of the overpotential

deposited nickel on a Au electrode, which indicates that the electrodeposited nickel is in the form of NiO (Ni^{2+}) as the peak at around 853 eV indicates [37]. Finally, the electrodeposited cobalt is in the chemical state of Co_3O_4 (as Co^{3+}) [38] as shown in Figure 2c.

3.2 Calculated adhesion energy of oxides on Au

To gain insight into the Au/oxide bonding we computed the adhesion energy of the three oxides identified in XAS (Cu_2O, NiO and Co_3O_4) on Au using both the oxygen terminated and metal terminated (111) surfaces, with the terminal oxide atoms over fcc hollow sites. In all cases the Au/metal terminated surface led to higher adhesion energies (see Table I). We also investigated metal terminated NiO and Cu_2O slabs adsorbed on hcp hollow sites, which were marginally higher in energy (more weakly bound).

If we focus only on the Au/metal terminated oxide interfaces the observed trend in adsorption energy can be rationalized as being due to the filling of the metal d-orbitals on the interfacial metal atoms. Figure 3a shows the project density of valence d states on the interfacial Au and metal atoms of the different oxides. The Au/Cu_2O interface can be seen to be characterized by a rather narrow Cu d-band with nearly all the Cu d-states filled on the interfacial atoms. If, however, we focus on the sum of the d states of the Ni atoms at the Au/NiO interface we see that the spin minority states are only partially occupied while the spin majority states are fully occupied (Figure 3b). Thus, in this case the spin minority anti-bonding d-states on the interfacial Ni atoms are empty. The same trend is seen for the Au/Co_3O_4 interface (Figure 3c). Here we see that both spin channels are partially occupied. Thus, in this series Au/Co_3O_4 is characterized by the lowest population of anti-bonding states across the interface, resulting in the largest increase in interfacial adhesion. Thus, we see that while Au oxide bonding stabilizes all the systems, it has the most pronounced effect on Co_3O_4. While offering insight into the nature of the bonding, we stress that these calculated adhesion energies ignore the electrolyte and electric potential and thus do not give a direct prediction of the interfacial stability under the measurement conditions.

3.3 Electrochemical performance of the electrodeposited metal -oxides on Au

After the electrodeposition 10 mM KCl was continually flowed through the cell. The cyclic voltammograms of Au and the electrodeposited electrodes are shown in Figure 4. The reference CV (Figure 4a) shows the oxidation and reduction peaks of Au at around +0.5 V and +0.05 V, respectively, which agrees with previously reported values [39]. The CV of the Cu@Au electrode (Figure 4b) reveals three peaks during anodic polarization. They are ascribed to the transitions Cu^0 to Cu^+ at -0.2 V ($2Cu^+ + 2OH^- \rightarrow Cu_2O + H_2O$), Cu^+ to Cu^{2+} at +0.3 V ($Cu_2O + 2OH^- \rightarrow 2CuO + H_2O$) and to $CuO + H_2O \rightarrow Cu(OH)_2$ at +0.6 V, [40] respectively. At reverse cathodic polarization

there are prominent peaks at -0.3 V and -0.7 V associated with the reduction of Cu^{2+} to Cu^{+} and Cu^{+} to Cu^{0}, respectively (the reverse reactions of the peaks at -0.2 V and +0.3 V). Furthermore, the chemical state under different polarization biases was investigated by means of *operando* FY-XA spectroscopy. Figure 4b shows the Cu $L_{II,III}$-edges of the Cu@Au electrode polarized at different potentials. At OCV (Figure 4aI) the spectrum reveals the presence of Cu^{+} (peak at ~932 eV). After that, the sample was negatively polarized at -0.7 V (Figure 4aII). The XA spectra indicate the Cu^{+} nature of the electrodeposited material, presumably in the form of Cu_2O, which remains stable at this polarization. The presence of Cu^{2+} species can be excluded within the detection limit (submonolayer) of our setup. However, polarization at positive biases induces the formation of Cu^{2+} species, presumably in the form of CuO (Figure 4aIII). After some time at +0.9 V, the copper signal disappeares, indicating that this material corrodes and dissolves in the form of Cu^{2+} ions under anodic polarization.

Figure 4c shows the CV of the electrodeposited Ni@Au complex in 10 mM KCl. At anodic polarization it shows two peaks at -0.06 V and +0.72 V attributed to the oxidation from Ni^{0} to Ni^{2+} and from Ni^{2+} to Ni^{3+}, respectively. At cathodic polarization there are peaks at +0.35 V and -0.42 V related to the reduction from Ni^{3+} to Ni^{2+} and Ni^{2+} to Ni^{0}, respectively [41]. Figure 4c shows the Ni $L_{II,III}$-edges XAS collected in FY mode under different biases in 10 mM KCl. At OCV the spectra shown in Figure 4cI are related to Ni^{2+} species in the form of NiO [42]. When the sample is cathodically polarized at -0.40 V, the spectrum remains unaltered keeping its Ni^{2+} nature (Figure 4cII). Anodic polarization at +0.35 V yields no modification in the XA spectra (Figure 4cIII). However, at +0.70 V the disappearance of the Ni $L_{II,III}$-edges (Figure 4cIV) reveals that the sample corrodes and dissolves in the electrolyte.

Finally, Figure 4d shows the CV of the electrodeposited Co@Au electrode. During the positive scan three oxidation peaks are assigned at -0.35 V, 0 V and +0.6 V. These peaks correspond to the Co^{0} to Co^{2+}, Co^{2+} to Co^{3+} and Co^{3+} to Co^{4+} transitions, respectively. During the negative potential scan the three peaks at +0.57 V, +0.16 V and -0.68 V are related to the Co^{4+} to Co^{3+}, Co^{3+} to Co^{2+} and Co^{2+} to Co^{0} reductions, respectively [43]. Figure 4d shows the $L_{II,III}$-edges of Co at different potentials. At OCV the spectrum shows a shape characteristic of Co_3O_4 (Co^{3+}) (see Figure 4dI) [44]. At -0.80 V the spectrum remains unaltered indicating that the electrode is stable under such conditions (see Figure 4dII). Finally at positive polarization at +0.70 V the electrode corrodes and dissolves as the vanishing of the Co $L_{II,III}$-edges in Figure 4dIII indicates.

Changes in the surface morphology were further investigated by means of *operando* EC-STM. This technique can be used to obtain atomically resolved *in situ* images of electrified interfaces under potential control in real time [45]. Using this approach we investigated the electrodeposition of Co on Au from 5 mM $CoSO_4$ solution and its

stability under reaction conditions in 10 mM KCl. Figure 5a shows the electrodeposition of cobalt on a Au foil at cathodic polarization (-1.0 V) showing that the surface undergoes morphological modification during the electrodeposition of cobalt. The polycrystalline Au foil used in this study was obtained from Alfa Aesar with a purity of 99.999 %. It had a roughness in the range of ~15 nm and grain size of around ~5 nm, These measurements were made at different elapse times: points I (0 s), II (180 s) and III (540 s). The surface of gold is decorated with particles in the range of tens of nanometers, as the bottom graphic (Figure 5a) indicated where the roughness and the grain size are plotted. After the electrodeposition of Co, the electrolyte was replaced by 10 mM KCl to investigate the morphological modification of the surface during anodic polarization at a fixed bias of +0.58 V, which revealed a modification of the surface most likely due to the oxidation/corrosion and dissolution of the electrodeposited material (see Figure 5b), as the measurements collected at different elapse times: points I (0 s), II (120 s) and III (260 s). The STM measurements show that the electrodeposited nanostructure vanishes, as indicated by a flatter gold surface morphology, as the bottom graphic associated to the roughness and grain size proves (Figure 5a). Consequently, the STM measurements agree with the information provided by the XA spectra and provide complementary information to the previous results. While higher resolution in the imaging can be achieved by the use of flatter surfaces, like single crystals, the investigation of the preferential sites of adsorption of the electrodeposited materials is out of the scope of the present work.

4. Discussion

In this work, the combination of advanced *operando* XA spectroscopy with potentiometric control in aqueous conditions showed trends in the stability and activity of electrodeposited Cu, Ni and Co (3d metals) on Au. These tendencies are summarized in Figure 6, which shows the trends in the cross- and overpotentials as well as total current at +1V vs. a Pt pseudo-reference electrode. It was found that the cross-potential, which corresponds to the equilibrium potential of the redox couple, becomes more negative with decreasing d orbital filling, yielding a $V_c(3d^{\lambda})>V_c(3d^{\lambda-1})$ relationship. For the $3d^n$ systems investigated here n is 10 for Cu, 8 for Ni and 7 for Co. This tendency is shown in the black curve in Figure 6, which indicates that the electrodeposition of copper requires a lower reduction potential than nickel and nickel lower than cobalt. On the other hand, the blue curve shows the decrease of the overpotential compared to a pure Au electrode (the overpotential was estimated at a current density of 10 mA/cm^2). It shows the same tendency $V_{OP}(3d^{\lambda})>V_{OP}(3d^{\lambda-1})$ as the cross-potential suggesting a relationship between these two parameters: A more negative cross-potential is associated with a lower overpotential. In order to compare the efficiency of these three electrodes, the current was measured at a potential of +1.0 V vs. Pt for each electrode, yielding the $I(3d^{\lambda})<I(3d^{\lambda-1})$ relationship between current density and 3d filling shown by the red curve. Thus, current follows the trends of the over- and cross- potentials. This indicates that electrodes that are “harder” to electrodeposit (higher negative cross-potential) yield higher current density and lower

overpotential as well as lower stability. It is interesting to note that the trends of the electrodeposited electrodes can be ascribed to their metal nobility [46], which suggest that the counter electrode can play an important role in the electrochemical performance, i. e. galvanic corrosion. However, this extreme remains as open question for future investigations.

The overall observed activity of the different composites correlates with interfacial bond strengths computed by way of DFT, see methods for details, which can be ascribed to the stabilization of the oxides afforded by adsorption on gold. The calculated adhesion energy of the various Au/oxide composites increases in the order $Cu_2O < NiO < Co_3O_4$ and is strongest when it is between Au and the metal-terminated oxide. The reason for the trend appears to be that Au/Cu_2O has bonding and anti-bonding d-states (on Cu) filled across the interface. Au/NiO has spin majority bonding and anti-bonding d-states filled across the interface but the spin minority anti-bonding d-states (on Ni) are not filled. Au/Co_3O_4 has empty anti-bonding d-states (on Co). While this gives insight into the Au/oxide bonding and the origin of the resultant lattice stabilization energy, we did not consider that under the conditions of the measurement the chemical potentials of the constituent atoms will likely make the system favor dissolution.

Dissolution was confirmed by XAS measurements, which clearly indicate that under anodic polarization the 3d transition metals corrode and dissolve in the electrolyte as ions. Thus, the total current under OER is due to a combination of water splitting and corrosion ($I_{total} = I_{OER}+I_{corrosion}$). In this case the electrodeposited materials do not work as catalysts, since they are consumed during the reaction process. Instead, they function as a sacrificial layer. Thus, the oxygen present in the transition metal oxide lattice must contribute to the overall reaction. Taking into account the oxidation state of the electrodeposited material, which was found by XA spectroscopy, the electrochemical reactions that take place at the different electrodes are described as follows. On a pure Au electrode we expect the water oxidation half reaction is:

$$2H_2O \rightarrow O_2+4H^++4e^-$$

Splitting two H_2O molecules requires the transfer of four electrons. The reaction that takes places on the electrodeposited Cu@Au electrode (which is in the form of CuO as the XAS measurements showed) is given as:

$$H_2O+CuO \rightarrow O_2+2H^++Cu^{2+}_{(aq.)}+4e^-$$

In this case, the oxidation of a single water molecule can be accomplished with $4e^-$ transfer because the reaction with the sacrificial layer of CuO yields Cu^{2+} ions that dissolve in the electrolyte. At the beginning, the Cu@Au electrode is in the form of Cu_2O and should be oxidized to CuO before its dissolution starts, which could explain why copper is more stable than nickel and cobalt. In the same direction, the

electrochemical water splitting reaction on the electrodeposited Ni@Au electrode (in the form of NiO as XAS measurements indicated) is described as:

$$H_2O+NiO \rightarrow O_2+2H^+ +Ni^{3+}_{(aq.)}+5e^-$$

In this case oxidizing a single water molecule involves the transfer of $5e^-$ yielding the reaction product of water splitting and dissolving the nickel into Ni^{3+} ions. Finally, Co@Au (in the form of Co_3O_4) is the most reactive electrode, as indicated by the highest current and lowest overpotential. The combined water oxidation and dissolution reactions can be described as:

$$2H_2O+Co_3O_4 \rightarrow 3O_2+4H^+ +3Co^{4+}_{(aq.)}+16e^-$$

This process involves the transfer of $16e^-$ to perform the decomposition of two molecules of water into its principal components yielding Co^{4+} ions as a subproduct of the reaction (corrosion process). Consequently, it was found that the ideal "snapshot" of these electrodes under OER is challenged by corrosion, which should not be noticed in massive bulky electrodes due to abundance of more active material in the bulk, but it is evident for thinner ones like in the present work. Therefore, the electrochemical activity reported for the transition metals on Au under OER conditions is strongly related to the lack of stability shown by these composites. Furthermore, the overpotential is directly associated with the cross-potential, which indicates that the electrochemical water splitting is most favored in materials with more negative deposition potentials. Meanwhile, under cathodic polarization these materials are stable. Consequently, this approach can be used to combine the electrocatalytic properties of several transition metals (including several metals in the same electrode) to produce more active and stable catalysts under cathodic polarization. Reactions like HER or the cathodic reduction of CO_2 are of special interest and electrodeposition offers the opportunity to effectively control the oxidation state of these catalysts, which opens up the way to design more complex electrodes including different materials to accomplish the desired reaction.

5. Conclusion

The activity and stability of electrodeposited transition metal oxides on gold for its use as electrocatalyst in the water splitting reaction was investigated by means of *operando* soft X-ray absorption spectroscopy in fluorescence yield mode. In order to accomplish these measurements, the 3d transition metals Cu, Ni and Co were electrodeposited on Au electrodes. Advanced *operando* XA spectroscopy revealed the oxidation state of the electrodeposited materials. Furthermore, the stability of these electrodes was inquired by XAS using an electrolyte free of OH^- and H^+ groups characteristic of alkaline and acidic media. Thus, 10 mM KCl was flowed in the cell to accomplish XAS measurements under reaction conditions at different polarizations. We establish that the overall activity of these electrodes is directly related to the

electrodeposition potential, i.e. to the cross-potential, which is associated with the equilibrium potential of the redox couple (dissolved ions and electrodeposited metal). In short, the activity observed is correlated with the lattice stabilization energy and the redox potential, which is at the origin of the incipient oxidation-corrosion resistance. Therefore, potentiometric methods alone used to describe the catalytic activity are not sufficient to distinguish between the current produced by the OER and the concomitant corrosion processes. The corrosion process is likely the origin of the activity reported for these composites, hence their sacrificial nature. To conclude we note that the role of the OH groups in the overall reaction/stability performance is missing in this investigation. To detect OH groups, other spectroscopic techniques, such as infra-red spectroscopy, should be applied. It remains as an open question for further investigations, which should reveal the role of these species in the electrocatalytic activity and stability observed.

Acknowledgements

We thank the Ministry of Education and Science of the Russian Federation (agreement #14.616.21.0007) and the Bundesministerium für Bildung und Forschung (project #05K2014) for financial support in the framework of the joint Russian-German research project “SYnchrotron and NEutron STudies for Energy Storage (SYNESTESia)”. We thank DAAD for financial support in the framework of Taiwanese-German collaboration (project ID 57218279). C.H.C. acknowledges financial support from projects 104-2112-M-032-005-MY2, 105-2911-I-032-501, 103-2112-M-032-004 and 102-2632-M-032-001 -MY3. We gratefully acknowledge the Höchst-Leistungs-Rechenzentrum Stuttgart (HLRS) for computational resources. T. E. J. acknowledges the Alexander-von-Humboldt foundation for financial support.

References

[1] Burke L D, and Nugent P F 1998.Gold Bulletin **31(2)** 39
[2] Rodriguez J A, Senanayake S D, Stacchiola D, Liu P. and Hrbek J 2013 *Accounts of chemical research* **47(3)** 773
[3] Haruta, M. 2002 *Cattech* **6(3)** 102
[4] Rodríguez J A, Feria L, Jirsak T, Takahashi Y, Nakamura K, and Illas F 2010 *Journal of the American Chemical Society* **132(9)** 3177
[5] Fu Q, Saltsburg H, and Flytzani-Stephanopoulos M 2003 *Science* **301(5635)** 935
[6] Rodriguez J A, Ma S, Liu P, Hrbek J, Evans J, and Perez M 2007 *Science* **318(5857)** 1757
[7] Zhou X, Xu W, Liu G, Panda D, Chen P 2009 *JACS* **132(1)** 138
[8] Brenner A 2013 *Electrodeposition of alloys: principles and practice*. London Elsevier.
[9] Velasco-Velez J J, et al. 2015 Angewante Chemie International Edition **54(48)** 14554
[10] Itkis D M, Velasco-Velez J J, Knop-Gericke A, Vyalikh A, Avdeev M, V, and

Yashina L 2015 ChemElectroChem **2(10)** 1427
[11] Guo J, Tong T, Svec L, Go J, Dong C, and Chiou J W 2007 *Journal of Vacuum Science & Technology A* **25(4)** 1231
[12] Jiang P, Chen J L, Borondics F, Glans P A, West M W, Chang C L, Salmeron M, and Guo J 2010. *Electrochemistry Communications* **12(6)** 820
[13] Hickling A., Hill S. Oxygen Overvoltage. 1947 *Discuss. Faraday Soc.* **1** 236
[14] Ruetschi P, Delahay, P 1955 *J. Chem. Phys.* **23(3)** 556
[15]Trasatti S1980 *J. Electroanal. Chem. Interfacial Electrochem* **111**, 125
[16] Lyons M E G, Brandon M. P. A, 2010 *J. Electroanal. Chem.* **641**, 119
[17] Man I C, Su H Y, Calle-Vallejo F, Hansen H , Martínez J I, Inoglu N G, Kitchin J, Jaramillo T F, Nørskov J K, Rossmeisl, J 2011, *ChemCatChem* 2011, **3 (7)** 1159
[18] Suntivich J, May K J, Gasteiger H A, Goodenough J B, Shao-Horn Y 2011 *Science* **334 (6061)** 1383
[19] Subbaraman R Et al. 2012 *Nature materials* **11(6)** 550
[20] Calle-Vallejo F, Díaz-Morales, O A, Kolb M J, Koper M TM, 2015 *ACS Catal.* **5 (2)** 869
[21] Burke M S, Enman L J, Batchellor A S, Zou S, Boettcher S W. 2015 *Chemistry of Materials* **27(22)**, 7549
[22] Papadimitriou S, Tegou A, Pavlidou E, Armyanov S, Valova E, Kokkinidis G, and Sotiropoulos S 2008 *Electrochimica Acta* **53(22)** 6559
[23] Velasco-Velez J J, Chuang C H, Han H L, Martin-Fernandez I, Martinez C, Pong W F, Shen Y R, Guo J, and Salmeron M 2013 *Journal of The Electrochemical Society* **160(9)** C445
[24] Velasco-Velez J J, Wu C H, Wang B Y, Sun Y, Zhang Y, Guo J H, and Salmeron M 2014 *The Journal of Physical Chemistry C* **118(44)** 25456
[25] Velasco-Velez J J, Wu C H, Pascal T A, Wan L F, Guo J, Prendergast D, and Salmeron M 2014 *Science* **346(6211)** 831
[26] Tröger L, Arvanitis D, Baberschke K, Michaelis H, Grimm U, and Zschech E 1992 *Physical Review B* **46(6)** 3283
[27] Perdew J P, Burke K, and Ernzerhof M, *Phys. Rev. Lett.* **1997**, *78*, 1396-1396.
[28] Giannozzi P et al. 2009 *J.Phys.: Cond. Matter* **21** 395502
[29] Dal Corso A 2014 *Comp. Mat. Sci.* **95** 337
[30] Marzari N, Vanderbilt D, De Vita A, and Payne M C 1999 *Phys. Rev. Lett.* 82 3296
[31] Cococcioni M, and de Gironcoli S 2005 *Phys. Rev. B* **71** 035105
[32] Chen J, Wu X, and Selloni A 2011 *Phys. Rev. B* **83** 245204
[33] Palomar-Pardavé M, González I, Soto A B, and Arce E M 1998 *Journal of Electroanalytical Chemistry* **443(1)** 125
[34] Fletcher S, Halliday C S, Gates D, Westcott M, Lwin T, and Nelson G 1983 *Journal of electroanalytical chemistry and interfacial electrochemistry* **159(2)** 267
[35] Dakkouri A S (997*Solid State Ionics* **94(1)**, 99
[36] Giesen M, Kolb D M 2000 *Surface science* **468(1)** 149

[37] Wang H et al. 2000 *Journal of the American Chemical Society* **122(43)** 10544
[38] Liang Y, Wang H, Zhou J, Li Y, Wang J, Regier T, and Dai H 2012 *Journal of the American Chemical Society* **134(7)** 3517
[39] Vitus C M, and Davenport A J 1994 *Journal of The Electrochemical Society* **141(5)** 1291
[40] Jayalakshmi M, and Balasubramanian K 2008 *Int. J. Electrochem. Sci.* **3** 1277
[41] Li M, Bo X, Mu Z, Zhang Y, and Guo L 2014 *Sensors and Actuators B: Chemical* **192** 261
[42] Regan T J, Ohldag H, Stamm C, Nolting F, Lüning J, Stöhr J, and White R L 2001 *Physical Review B* **64(21)** 214422
[43] Casella I G, and Guascito M R 1999 *Electrochimica Acta* **45(7)** 1113
[44] Papaefthimiou V et al., 2011 *ACS nano* **5(3)** 2182
[45] Chen C. J. 2008 *Introduction to scanning tunneling microscopy*. Oxford University Press
[46] Ghali E, Sastri V S, Elboujdaini . 2007 *Corrosion prevention and protection: practical solutions.* John Wiley & Sons.

Table I: Adhesion energies computed at the PBE_U level, see text for details

System	Oxygen fcc [meV/Å^2]	metal fcc [meV/Å^2]	metal hcp [meV/Å^2]
Cu_2O	-27	-100	-94
NiO	-114	-153	-140
Co_3O_4	-216	-226	----

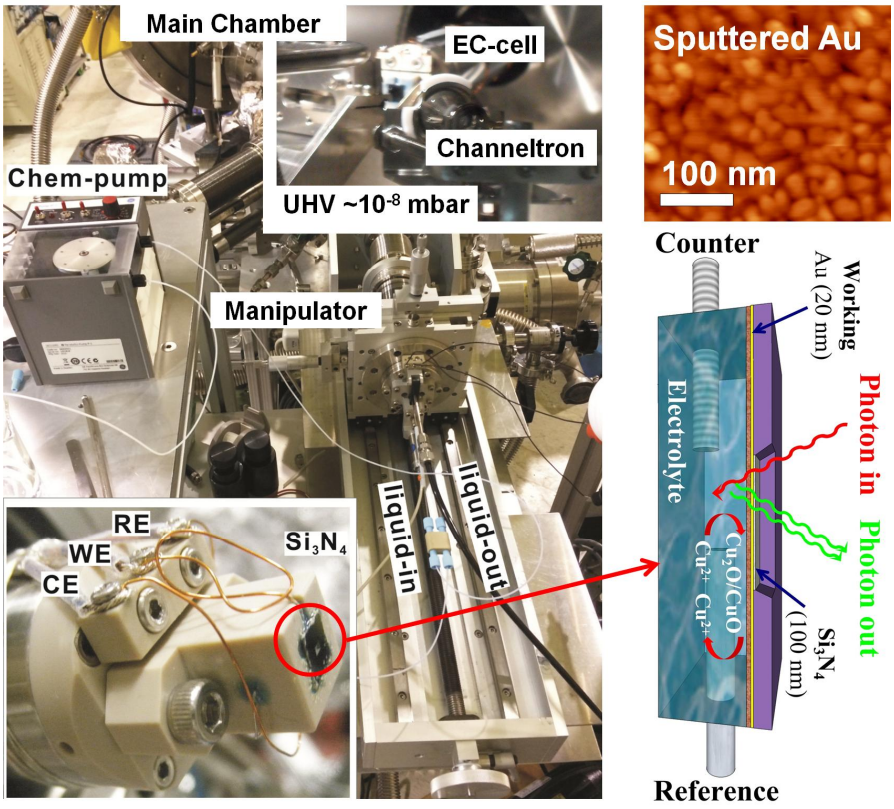

Figure 1: Pictures of the operando electrochemical XAS cell installed at the beamline 20A1 of the NSRRC (Taiwan) and the detection schema by means of FY-XAS using a thin SiN_x membrane to separate the UHV in the main chamber from the aqueous electrolyte. The AFM image shows the sputtered 20 nm Au on the SiN_x membrane used as electrode.

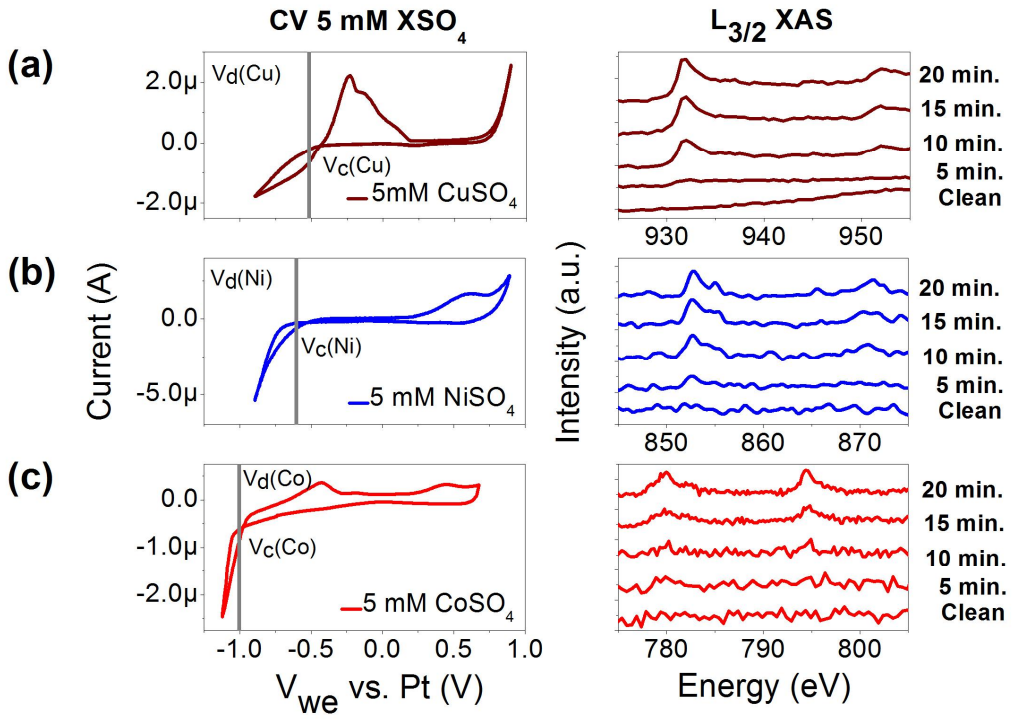

Figure 2: CVs collected with the Au working, Pt counter and Pt pseudo-reference electrodes and the XA spectra (as a function of time) collected under working conditions. The electrolytes used are 5 mM $CuSO_4$, $NiSO_4$ and $CoSO_4$. a) XA spectra of Cu L_{II-III}-edges collected at -0.5 V in 5 mM $CuSO_4$. b) XA spectra of Ni L-edge collected at -0.6 V in 5 mM NiSO4. b) XA spectra of Co L_{II-III}-edges collected at -1.0 V in 5 mM CoSO

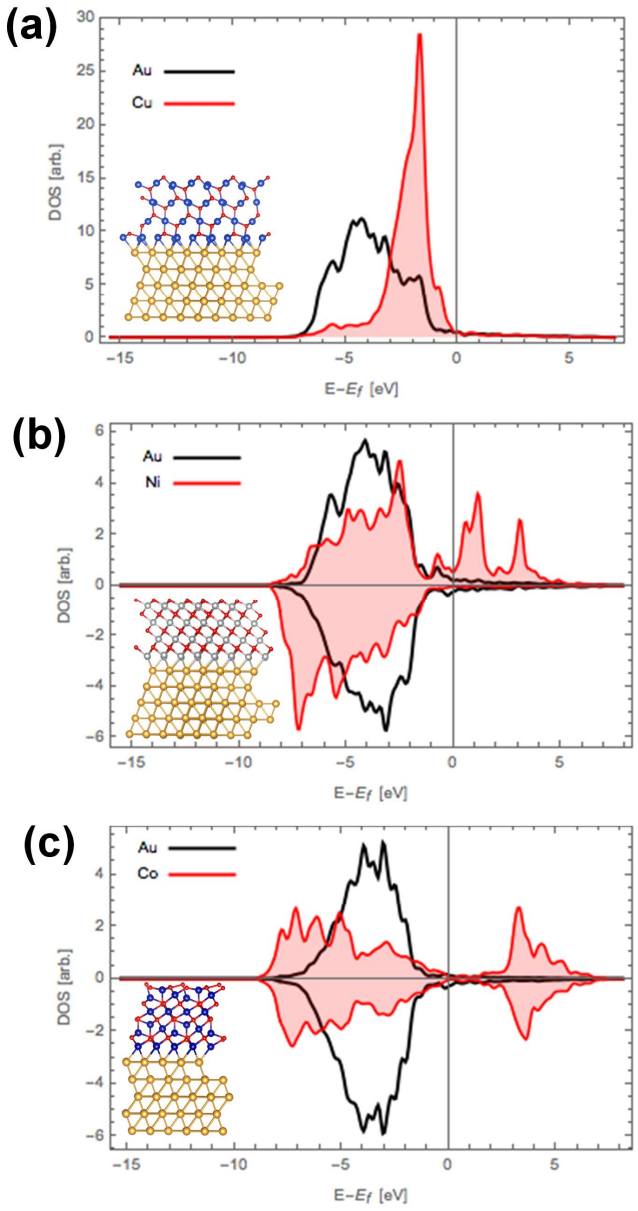

4.

Figure 3: (a) $Cu_2O(111)/Au(111)$ d-states projected on interface atoms (Au/Cu). Inset: Metal terminated $Cu_2O(111)/Au((111)$ interface structure (Copper atoms are blue, oxygen red, and gold yellow). (b) NiO(111)/Au(111) d states projected on interface atoms (Au/Ni). Inset: Metal terminated NiO(111)/Au(111) interface structure (Ni atoms are shown as silver, oxygen red, and gold yellow). (c) $Co_3O_4(111)/Au(111)$ d-states projected on interface atoms (Au/Co). Inset: Metal terminated $Co_3O_4(111)/Au(111)$ interface structure (Co atoms are shown as blue, oxygen red, and gold yellow).

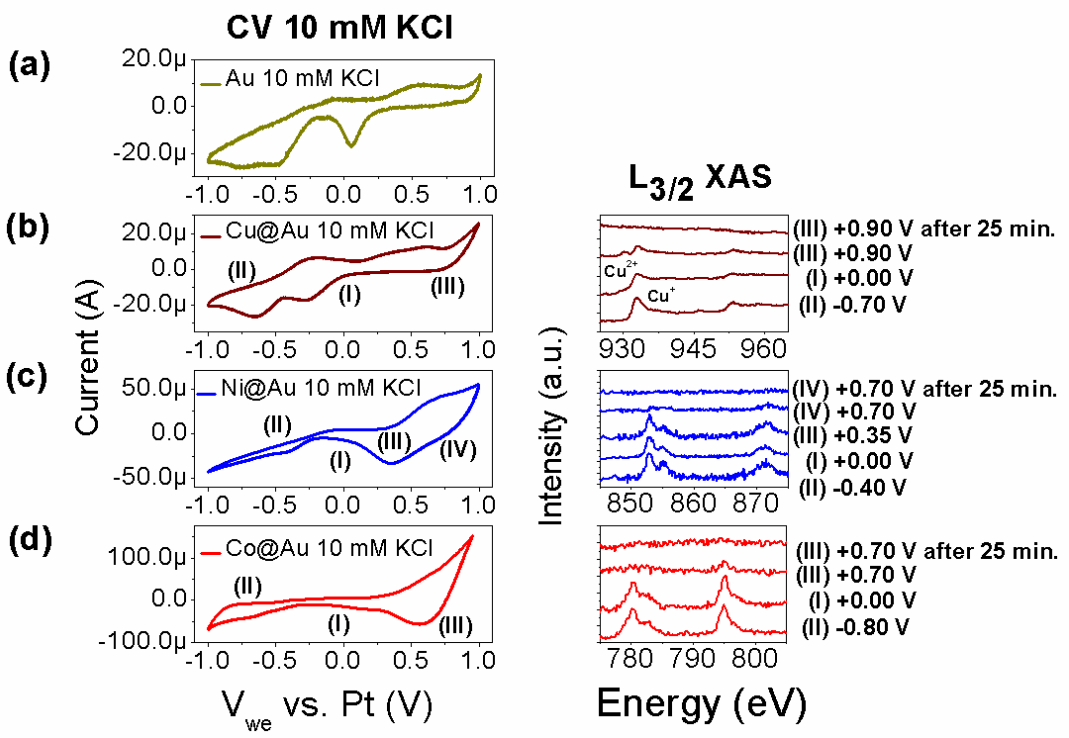

Figure 4: CVs collected with Au, Cu@Au, Ni@Au and Co@Au working electrodes (Pt counter and Pt pseudo-reference electrodes). The electrolyte is 10 mM KCl. a) CV collected from pristine Au electrode b) CV collected with Cu@Au electrode and XA spectra of Cu L_{II-III}-edges at several biases in 10 mM KCl. c) CV collected with Ni@Au electrode, XA spectra of Ni L_{II-III}-edges at several biases in 10 mM KCl. d) CV collected with Co@Au electrode, XA spectra of Co L_{II-III}-edges at several biases in 10 mM KCl.

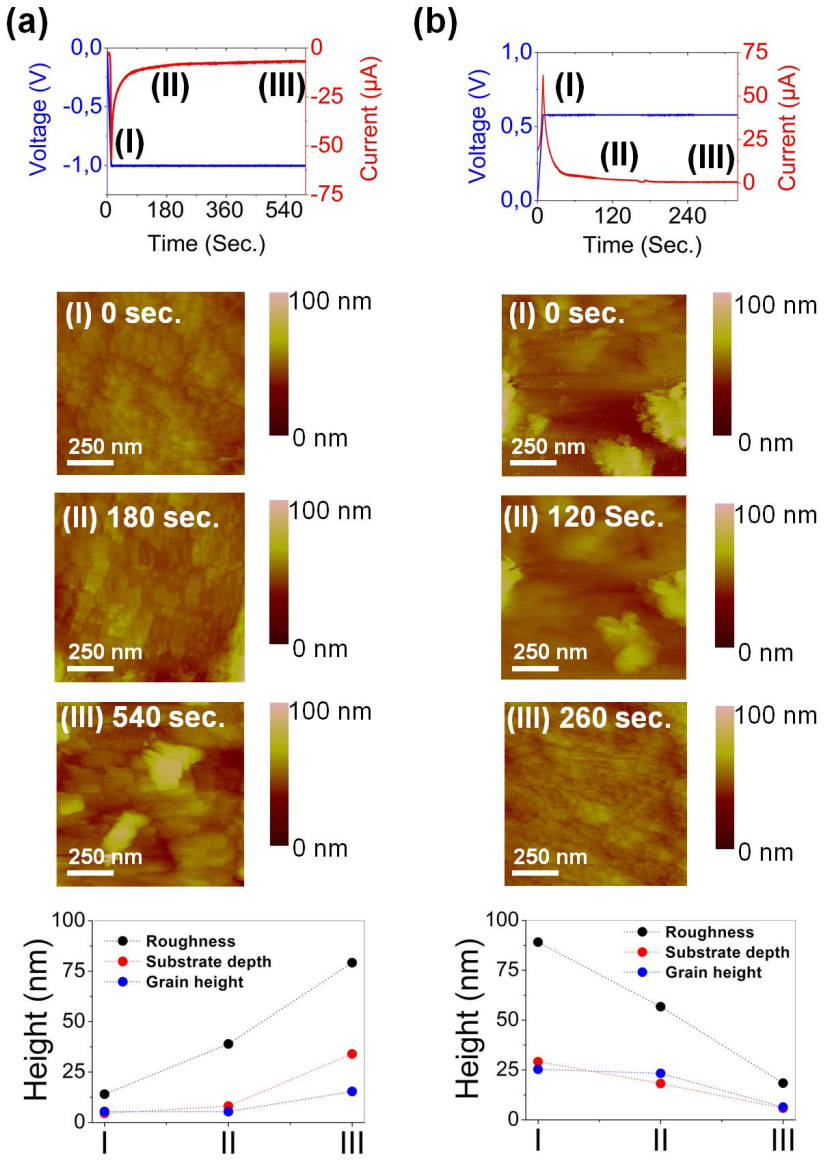

Figure 5: a) STM measurements of the electrodepositions of Co on Au at -1.0 V from 5 mM $CoSO_4$ with Pt as counter and reference electrodes including the potential and current vs time (top) and the changes in the roughness and grain sizes (bottom). b) STM measurements of the electrodeposited Co@Au composited at +0.58 V in 10 mM KCl including the potential and current vs time (top) and the changes in the roughness and grain sizes (bottom).

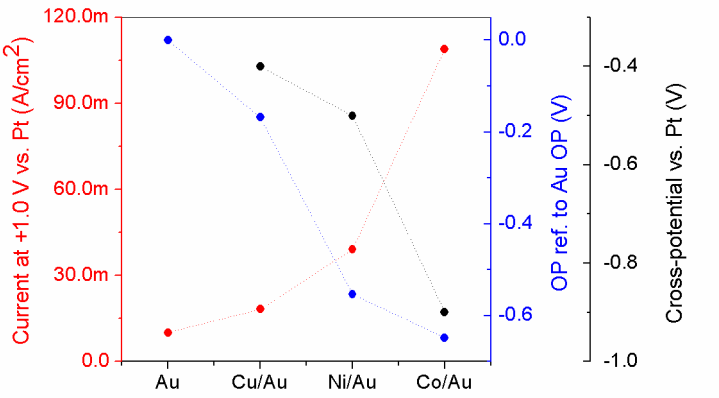

Figure 6: Electrode trends of the principal parameters such as cross-potential, overpotential referenced to Au and current density at +1.0 V for Au, Cu@Au, Ni@Au and Co@Au electrodes.